Isothermal Temperature Control for Battery Testing and Battery Model Parameterization

Alister Hales, Etienne Brouillet, Zhihou Wang, Blair Edwards, Mohammad Amin Samieian, Jake Kay, Stelios Mores, Daniel Auger, Yatish Patel and Gregory Offer

Abstract

The hybrid/ electric vehicle (H/EV) market is very dependent on battery models. Battery models inform cell and battery pack design, critical in online battery management systems and can be used as predictive tools to maximise the lifetime of a battery pack. Battery models require parameterization, through experimentation. Temperature affects every aspect of a battery's operation and must therefore be closely controlled throughout all battery experiments. Today, the private-sector prefers climate chambers for experimental thermal control. However, evidence suggests that climate chambers are unable to adequately control the surface temperature of a battery under test. In this study, laboratory apparatus is introduced that controls the temperature of any exposed surface of a battery through conduction. Pulse discharge tests, temperature step change tests and driving cycle tests are used to compare the performance of this conductive temperature control apparatus (CTCA) against a climate chamber across a range of scenarios. The CTCA outperforms the climate chamber in all tests. In CTCA testing, the rate of heat removal from the cell is increased by two orders of magnitude. The CTCA eliminates error due to cell surface temperature rise, which is inherent to climate chamber testing due to insufficient heat removal rates from a cell under test. The CTCA can reduce the time taken to conduct entropic parameterization of a cell by almost 10 days, a 70% reduction in the presented case. Presently, the H/EV industry's reliance on climate chambers is impacting the accuracy of all battery models. The industry must move away from the flawed concept of convective cooling during battery parameterization.

1

Keywords

Lithium-ion battery, battery testing, battery model parameterization, isothermal battery testing, climate chambers, conductive cooling, convection cooling, temperature control, temperature boundary conditions

Introduction

The hybrid/ electric vehicle (H/EV) market is expected to triple in the next decade [1]. Research must drive innovation and advancement across the H/EV industry, to match the anticipated demand for alternative powertrains in the automotive sector. Lithium-ion cells represent the most promising solution for the energy source in H/EVs with all major automotive companies investing in an imminent lithium-ion future [2], [3]. Policy incentives have been introduced in countries around the world, aiming to accelerate the global shift towards transport electrification [4]–[6].

Battery Modelling

Numerical battery models are used to evaluate a battery's behaviour in a variety of conditions, for example as operating temperature and power demand are varied. Each variance of the conditions is referred to as a 'usage-case', whilst the 'battery' that is being modelled may refer to a single lithium-ion cell or an entire battery pack. Battery models, in their various forms, are central to the design and operation of every battery pack that exists in the H/EV industry today. Usage-cases are imposed on the battery model, and the outputs from the model are used to approximate the anticipated behaviour of the battery. The anticipated behaviour is used to inform the designer about performance, longevity and the operating conditions that will optimise lifetime operation.

There are two main types of battery models: physics-based models and electrical equivalent circuit models (ECMs) [7], [8]. ECMs simulate a battery's behaviour by modelling resistors, capacitors and voltage sources in a circuit and can range in complexity [8]. ECMs are less

2

computationally demanding than physics-based models. In the H/EV industry, this allows the model to run in real-time, often embedded in a microprocessor within the ECU [7], [9]. As a result, ECMs are the most common type of battery model used in the industry today.

Thermal models are often coupled with ECMs. Thermal models describe heat generation and heat transfer that occurs within a model domain. The model domain may be a localised site in a single cell, or an entire battery pack [10], [11]. They are an essential component of battery modelling because temperature affects every aspect of a cell and pack operation [12]–[15]. Thermal models are employed and coupled with ECMs when steady temperature conditions cannot be assumed. This is true for all high-rate applications because of significant heat generation rates, as found across the H/EV industry [16]–[18]. The impact of temperature dependent operation is most evident at low temperatures, where magnitude of heat generation is greater because cell resistance is higher [12], [19].

Battery models are employed throughout the lifecycle of a battery pack [11]. In the pre-prototype phase of battery pack design, battery models are used to predict and compare the expected performance of cells and packs in operation [20]. Battery models are also used to inform the design of a battery pack's thermal management system (TMS), providing heat rate inputs into CFD solvers [21]. Onboard battery management systems (BMSs) are used to ensure safe and optimal operation of a battery pack over its lifetime. BMSs require low computational, simple battery models in order to approximate the battery's performance in real-time [22], [23]. Increasingly, the H/EV industry is implementing digital twin technology, where the operation of a battery pack on the road is mimicked through computation in real-time [24], [25]. The 'digital twin' assesses the performance variation of a battery pack from beginning-of-life to end-of-life, and is used as a tool to extend lifetime [26], [27]. Battery models are central to all digital twin technology. Without accurate simulation of battery pack performance, the data produced by the digital twin is flawed.

Battery Model Parameterization

The parameterization method is a key component to any battery model. Parameterization defines the use of experimental data to calibrate the battery model. For example, the resistance and capacitance of every resistor and capacitor in an ECM must be determined. Accurate parameterization is very important. An inaccurately parameterised model will incorrectly approximate the performance of the battery which it is designed to represent [12], [28]. Cell manufacturers rarely publicise a given cell's composition of assembly. As a result, experimental parameterization is often the only method available for the designers of battery models.

Electrochemical Impedance Spectroscopy (EIS) has historically been the most common method for ECM parameterization [12], [29], [30]. However, EIS requires specialist testing equipment which renders the technique inaccessible to many, particularly in the private-sector. Pulse discharge (PD) testing provides an alternative model parameterization technique which can be carried out on any cell cycler [16]. A PD test involves a repetition of constant current discharge 'pulses' followed by extended relaxation periods, from 100% SOC to 0% SOC. The key to PD parameterization is the relaxation of the measured voltage. Following each current pulse, the measured voltage will return to the cell's open-circuit voltage (OCV). The rate and nature of this relaxation is used to approximate electrochemical properties of the cell. As a battery's electrochemical properties vary significantly with temperature, PD discharges must be conducted across a wide range of temperatures.

Zhao *et al.* introduced the following experimental procedure, repeating the PD at 10°C, 20°C, 30°C and 40°C [16], [31]. Figure 1 shows the current input and the voltage response from the defined PD procedure.

1. 100% - 90% SOC discharge, in 1% ΔSOC increments at 1C discharge rate, 2-hour rest following each pulse

2. 90% – 20% SOC discharge, in 5% ΔSOC increments at 1C discharge rate, 2-hour rest following each pulse

3. 20% - 0% SOC discharge, in 2% ΔSOC increments at 1C discharge rate, 2-hour rest following each pulse

The rest times in this procedure are substantial, 2 hours long, because the cell must be given sufficient time to relax between each pulse [32]: the nature of this relaxation is required for ECM parametrisation. Measured cell voltage is itself dependent on cell temperature, and therefore temperature during relaxation is also an important consideration.

Thermal models typically need a heat generation input. Heat generation of a cell can be split in two: irreversible and reversible [19], [33]. Approximation of reversible, entropic, heat generation requires experimentation [34]. The entropy change as a function of SOC change is required across a wide range of temperatures [17]. This is found by evaluating the change relative to the cell OCV, as a result of SOC and temperature variation. Zhao *et al.* introduced the following experimental procedure to measure entropy change [16], [31].

1. Cell initially at rest, at 100% SOC

2. Cell temperature set to 15°C

3. 4% ΔSOC constant current discharge at C/20

4. 4-hour rest

5. 5°C temperature rise of cell boundary conditions

6. 4-hour rest

    a. Return to step 5 until 40°C has been reached

    b. Return to step 2 until 0% SOC has been reached

The rest times in this procedure are significant because the measured cell voltage must be given an extended period to reach OCV. This rest time is heavily affected by the speed at which the change to cell temperature (step 3a) can be imposed.

A coupled electro-thermal model must be validated against experimentation. In validation, the same driving cycle is run in the model and in an experimentation. The World Light Test Procedure Class 3 cycle is a commonly used driving cycle in the H/EV industry [35]. Selected measurable parameters, such as cell voltage and temperature, are recorded from the simulation and the experiment. The results are compared and the model's performance and capability is based upon how well they correspond. The thermal boundary conditions for such experiments are very important, isothermal conditions are typically preferred [16], [29], [30], [36].

Temperature in Battery Model Parameterization

Temperature and temperature gradients affect every aspect of lithium-ion cell operation, and this has a considerable effect on cell parameterization. Troxler *et al.* parameterised an ECM using EIS data across a wide temperature range; the fitted cell series resistance values increase by approximately 750% as the temperature is reduced from 55 °C to -5°C [13]. Therefore, temperature must be controlled throughout parameterization and validation experiments to mitigate the effects of such temperature dependent performance variation.

Temperature control is complicated because of electrochemical heat generation, which occurs in every lithium-ion cell. In the H/EV industry, PD parameterization is often conducted at a rate of 1C, whilst driving cycles will regularly demand power in excess of 1C. At these rates, heat generation is significant [31], [37]–[40]. Perfect temperature control of a lithium-ion cell is not possible because active cooling can only be applied onto the external surfaces of the cell. Therefore, the build-up of temperature gradients within a cell are inevitable, as the heat generated inconsistently and nonuniformly within its volume is conducted to the cooled surface(s). In most applications of parameterization, optimal thermal control would be achieved through entirely uniform temperature across the entire exposed surface of the cell. Advanced modelling techniques have been explored and developed to quantify the temperature gradients within the volume of the cell [41], [42]. Such methods complement experimental data which aims to achieve isothermal conditions on a cell surface.

6

Climate chambers are the most common thermal control systems for cell parameterization [29], [30], [43]. They are widely used across academia and the private-sector. Forced convection, generated through fans in the climate chamber, is used to cool exposed cell surfaces. Chamber temperature is controlled by circulating the contained air through a heat exchanger, set to a desired temperature by the operator. Climate chamber popularity is easy to understand. For low hazard testing, climate chambers are inexpensive and a single climate chamber can be used for a whole range of cell parameterization tests. They are able to accommodate a wide variety of cells, from small coin cells up to large prismatic cells. Climate chambers allow easy access for the experimentalist with minimal additional apparatus required for safe and repeatably lithium-ion cell testing.

Climate chambers have a very significant drawback: they are unable to effectively control the temperature of a cell during testing when significant cell heat generation is expected. Ardani *et al.* [12] tested climate chamber performance through routine experiments: a 2C discharge of a 5Ah *Kokam* pouch cell for 12 minutes, with temperature varied between 5°C and 45°C. Table 1 summarises the key findings. The temperature of the cell surface rose 5.7°C over the course of the test conducted at 5°C. Ardani proposed to solve the convective cooling limitations by using conductive cooling [12]. Table 1 displays further results from the same set of study, this time with small cooling blocks mounted to the cell surface to induce conductive cooling. The temperature deviation from the desired reduces by approximately 75% for each test.

The impact of the different cooling methods on the cell parameterization procedure is also published [12]. Datasets from complete cell parameterization procedures, using either a climate chamber or conduction apparatus for temperature control, were used to parameterise a battery model [34]. The resulting models' performances differed considerably. For example, the sub-ambient diffusion coefficient of the cathode, was estimated through the model to be around four times larger when the climate chamber data was used, compared to the conduction apparatus. The cathode charge transfer coefficient

was estimated to be around 50% larger when convection cooling data was used. The fitted parameters are highly dependent on the temperature at which they were determined in the parameterization experiments. The evidence reaffirms that good temperature control is essential for good battery model parameterization in the H/EV industry.

Objectives

In this paper, we introduce conductive thermal control apparatus (CTCA). The CTCA has been designed to overcome the limitations that have been introduced with existing temperature control techniques. We will analyse the thermal control performance of the CTCA for a range of experiments devised to replicate typical cell parameterization that would be observed in academia and the private sector. All results will be directly compared to equivalent sets of data recorded through testing in an industry-standard climate chamber.

Experiments

Cell

The cell used in testing is anonymous for confidentiality reasons. The cell is designed for automotive applications and has a 56Ah capacity. It is a pouch cell with both tabs located at one end of the pouch. The electrode-stack has a total length of 240mm and a total width of 200mm. The electrode-stack is contained by a pouch material, typical across the battery industry, made from polymer-laminated aluminium foil. The cell model has a $LiMnNiCoO_2$ (NMC) cathode and graphite anode, chemistry typical within the lithium-ion battery industry. Two cells were used in testing, one in the CTCA (Cell CTCA) and the other in the climate chamber (Cell CC). Both cells completed 10 cycles across their voltage range before testing begun. A C/40 discharge was conducted at 25°C on each cell to ensure accessible capacity in each was equal. Their capacities deviated by 0.3%, 55.37 Ah in the climate chamber and 55.19 Ah in the CTCA.

Conductive Thermal Control Apparatus

The CTCA is a temperature control apparatus that employs conductive cooling to achieve highly accurate temperature control during lithium-ion cell testing. A high-level schematic of the CTCA is shown in Figure 2. The CTCA consists of a Cell Test Area, a Heat Removal System and a Control System.

The CTCA removes heat from the cell test area using high levels of turbulence in the coolant fluid flow, which is recirculated through a cooling coil. The cooling coil removes heat from the coolant fluid through a refrigeration cycle, which may provide up to 3.5 kW of cooling. A control system drives the refrigeration cycle, which is used to maintain the temperature of the coolant fluid at a prescribed temperature; typically 1°C below the cell temperature setpoint. A dielectric silicon oil (*Dow Syltherm HF*) is used as the coolant fluid in this testing, although any dielectric coolant may be used. The coolant fluid is driven around the CTCA and through the Cell Test Area using two propellers immersed in the fluid.

A schematic of the cell test area is shown in Figure 3 and the arrangement of cooling modules on the top surface of the tested cell is shown in Figure 4; the arrangement is identical for the bottom surface. An image of the pouch cell under test, setup within the cell test area, is shown in Figure 5. The tabs are connected to the cell cycler through copper clamps. Cooling modules, mounted on the copper clamps, enable tab temperature control.

Each copper cooling module contains a Peltier element and a N-type thermocouple. Each cooling module is 100 mm x 80 mm, with a thickness of 5 mm. As such, the six cooling modules entirely cover a single surface of the cell. The thermocouple is located at the centre point of the cooling module surface, 1mm from the surface of the cell (annotated in Figure 3 and Figure 4). The cooling modules are able to withstand a maximum pressure of 0.3 MPa, such that compression may be placed onto the test cell during experimentation. Therefore, six cooling modules are required to cover each surface of the test cell, and a further cooling module is required for each tab. Each Peltier element is able to deliver 100 W of heat

removal when a 0°C temperature gradient exists across it, generating 250 W of waste heat. The control system, which aims to set the temperature of the cell surface to a prescribed temperature, uses the thermocouple as feedback into the PID control software. The heat from the cell is rejected through the outer surface of each copper cooling module and into the coolant fluid contained within the heat removal system. Each cooling module is held on the cell's surface by a frame constructed around the cell test area.

Apparatus

A *KB53 BINDER* climate chamber was used in all tests; its performance capabilities are typical of the many different climate chambers used across the battery industry. The *KB53* was new at the start of this investigation and is the latest generation produced by *BINDER* (as of 1st August 2020). The specification sheet states the chamber is operational between -10 °C and 100 °C and is able to achieve ±0.1 °C temperature stability at 37 °C. The internal volume of the chamber is 53 L (width: 0.4 m, height: 0.4 m, depth: 0.33 m) [44]. In all tests, the cell was positioned without confinement on a wire rack in the centre of the chamber's volume. Cables to the cell cycler exited the climate chamber through a sealed gland at the centre of the top face of the climate chamber. The climate chamber fan speed was set to 100% in all tests.

A *Maccor* cell cycler was used for each climate chamber test and a *Chroma* cell cycler was used for each CTCA test. Cell surface temperature was recorded at 12 sites on the cell surface, to match the locations of the temperature recording in the CTCA cooling modules. K-type thermocouples were used for all climate chamber tests, and temperature was logged through *Pico TC-08* hardware and *Picolog 6* software. N-type thermocouples were used for all CTCA tests, and temperature was logged through the CTCA hardware and software.

Methods

Three different sets of experiments were devised to assess the functionality of the CTCA against the industry-standard control apparatus, the climate chamber. In each set of

experiments, identical tests were conducted using the CTCA and the climate chamber. The aim in each test was to maintain uniform temperature conditions across the surfaces of the cell. In all tests, the average of all cell surface mounted thermocouples was taken and used to represent cell surface temperature.

In all tests, the cell was uncompressed. This was done because any externally applied compression would require additional apparatus within the climate chamber test setup, and as such affect the properties of the thermal system by adding thermal inertia. In the climate chamber, the cell was therefore entirely unconfined. In the CTCA, the cooling plates were compressed onto the cell surfaces, but with minimal force. Further to this, the external mounts for each cooling plate (Figure 5) allowed a small amount of movement along the axis normal to the plane of the cell surface. As such, expansion and contraction of the cell during cycling would not lead to varying compression of the test cell.

The tab clamps used in the climate chamber setup were manufactured from brass, whilst those used in the CTCA were copper. In the climate chamber, the voltage-sense cable was connected to the tabs through the clamps, whilst in the CTCA, the access allowed the voltage-sense to be connected directly onto the tabs. Further, different cell cyclers were used for the respective tests. During preliminary testing, it was found the change to measured cell voltage, from OCV and instances where current was being passed into or out of the cell, varied to a degree between the climate chamber tests and the CTCA. This variation is contributed to by the contact resistance, from clamp to tab, in the climate chamber setup causing a voltage drop when current was being passed through the interface. The impact of the different voltage sense-response (whilst charged was being passed) from each cell cycler may also contribute to the variation. For this reason, the voltage response analysis in this investigation (during pulse discharge testing) will focus solely on the periods where no current is being passed into and out of the cell.

Pulse discharge testing was conducted to assess the CTCA's ability to maintain isothermal temperature conditions during PD cell parameterization. Isothermal temperature conditions are essential for reliable cell characterisation. Table 2 shows the test matrix.

Temperature step change testing was conducted to assess the CTCA's ability to induce step change temperature conditions across the surfaces of the test cell. This type of boundary condition is essential for entropy change parameterization. Table 3 shows the test matrix.

Driving cycle testing was conducted to assess the CTCA's ability to maintain isothermal conditions during driving cycle loading on the test cells. The Worldwide Harmonised Light Vehicle Test Procedure, class 3 (WLTP) was used for all tests [35], [45], [46]. The driving cycle experienced by individual cells was determined with reference to vehicle speed and generated using a 'backwards-facing' approach using quasi-static representations of vehicle aerodynamic and mechanical resistances, together with an efficiency-based powertrain model incorporating a simple regenerative braking law. The velocity profile was taken from the *Driving Cycle* blockset (*MATLAB Simulink*) [47], and this was coupled to a bespoke Simulink model. The vehicle was modelled as small compact 'C segment' car weighing 1600 kg including payload and the power demands were scaled assuming 192 cells in a pack. Parameters were tuned to give a similar energy consumption to a known (pre-WLTP era) test case for a popular production vehicle [48]. For ease, uniform distribution of load across every cell in the pack was assumed. The power-rated load on a single 56 Ah cell is shown in Figure 6. The tests were conducted at 5 °C and 25 °C.

Results and Discussion

Pulse Discharge Testing

Pulse discharge testing allowed for direct comparison between 30 sets of climate chamber and CTCA data. Figure 7 compares the temperature rise and the voltage response following P2 (90% - 85% SOC pulse discharge) at 25°C. Noticeable temperature rise, above the

desired temperature, occurs on the surface of the cell in the climate chamber test, but not in the CTCA test. This deviation from the desired temperature is termed ΔT_{rise}. However, it is difficult to observe the effect of this temperature disparity through the voltage response alone. Therefore, the voltage derivative (dV/dt) is plotted in Figure 8, in order to assess the rate of voltage change during the settling period. It is evident that the cell voltage settling time is slightly longer in the CTCA test. This is in line with expectations: the temperature rise in the climate chamber test will reduce the cell impedance and consequently increase the rate of a return to equilibrium. In order to quantify the rate of return to equilibrium, for both cell voltage and cell surface temperature, threshold limits have been set for each. The cell is considered in equilibrium when $dV/dt < 10^{-6}$ V.s^{-1} and the $\Delta T_{rise} < 0.25°C$.

Test P2 at 25°C was repeated, including fully repeating the procedure to setup the apparatus for the respective tests, to evaluate the systematic error of the climate chamber and the CTCA. Results are also plotted in Figure 7 and Figure 8. In the climate chamber tests, the dV/dt settling time reduces by 4.4% and the temperature rise settling time reduces by 6.2%. In the CTCA tests, the dV/dt settling time is increased by 2.4% and the temperature rise limit was not breached in either test. These results highlight consistency of experiment in both setups, and suggest a slightly reduced level of systematic error in the CTCA setup.

The temperature data from each climate chamber P2 test is shown in Figure 9. The problem of temperature rise is exaggerated at low temperatures, both in terms of maximum temperature rise reached, $\Delta T_{rise\ max}$, and the time to settle. This is to be expected, since heat generation from the cell would be greater at low temperatures. The same trends are observed in all pulse discharge tests conducted. The results from these tests are included in Appendix A, A 1 and A 2.

Figure 10 represents the dV/dt settling time for each P2 test. In the 25°C, 35°C and 45°C tests, the dV/dt settling times in the CTCA tests deviate from the climate chamber tests by an average of 3.3%. However, with the pulse discharges at lower temperatures, the deviation noticeably increased; 11.5%, 19.8% and 22.4% at 15°C, 5°C and -5°C respectively. This

illustrates how, in the low temperature tests, the effect of temperature rise above the desired test temperature is exaggerated. In consequence, the cell voltage settles faster in the climate chamber since the cell temperature is higher than the desired set temperature. This extra heat reduces the cell impedance and increases the rate of return to the electrochemical equilibrium state of the cell. These observations are not unique to P2 tests. At 5°C, a 4.5% deviation is found in the P3 tests and a 15.4% difference is found in the P4 tests. When smaller pulse discharges such as P1 and P5 are studied, the temperature rise is dramatically reduced, leading to trivial differences between climate chamber and CTCA data. The dV/dt settling times for all tests conducted may be found in Appendix B, A 3 and A 4.

The effect of the climate chamber error is not limited to just settling times. There is also a clear deviation in the shape of the dV/dt data, particularly at lower temperatures. Figure 11 shows the 5°C, P4 test datasets. The shape of the dV/dt data from the climate chamber is changed because of the cell is not at the desired temperature during the voltage settling period. The data suggests that the dV/dt response in the climate chamber is affected by the temperature settling response. The cell's electrochemistry returns to near equilibrium before the temperature of the climate chamber cell is able to return to equilibrium, because of the less effective climate chamber cooling. As a result, the cell temperature change, even when at electrochemical equilibrium, is driving a continual change to cell voltage.

During pulse discharge testing, unwanted change to the cell surface temperature affects the voltage response of the cell. The problem is fundamentally caused by a climate chamber's inability to remove heat from a test cell at the required rate, and therefore the problem is exaggerated at low temperatures, where heat generation is greater. The effect of dV/dt relaxation deviation occurs because the cell impedance is affected by cell temperature, and once again this is most evident at low temperature. The climate chamber cell, across all tests, returns to equilibrium faster than the CTCA cell and the shape of the dV/dt relaxation is altered by the undesirable and uncontrollable ΔT_{rise}. Such climate chamber data is used commonly to parameterise battery models across the H/EV industry, where the cell

temperature is assumed to be constant throughout the cell voltage relaxation. This is incorrect and leads to parameterization error which is carried forward into the application of the battery model. As an example, many battery management algorithms make use of equivalent circuit network models with parameters representing, for example, voltages or resistances. When tests are done 'out of pack' with poor temperature regulation, the models obtained can differ significantly from the behaviours exhibited with good temperature regulation.

Temperature Step Change Testing

The temperature step change tests were conducted to see how effective the CTCA is at inducing a controlled step change in temperature upon the test cell's outer surfaces. Figure 12 shows the response when a step temperature change, from 25°C to 30°C, is implemented. A log scale had to be used on the time axis to refine the resolution of the CTCA response curve. The same temperature settling threshold as with the PD tests, $\Delta T <$ 0.25°C, is used here. In the climate chamber test, it takes the cell 75 minutes to reach this threshold. In the CTCA tests the settling time is reduced to 1.3 minutes. Across all tests with a 5°C step change, the CTCA response time is reduced by an average of 98%, compared to the climate chamber (1.6 minutes, compared to 84 minutes). In the 25°C temperature change tests, the climate chamber took 132 minutes to rise to 40°C and 140 minutes to fall to 15°C. In the CTCA, the step temperature rise took just 3.0 minutes and the temperature fall took 3.9 minutes, a reduction of 98% and 97%, respectively. All data relating to temperature step change testing is shown in the Appendix C, A 5 and A 6.

Figure 12 also shows the rate of cell surface temperature rise. In the climate chamber, a maximum rate of 0.0022 °C.s^{-1} is achieved. In the CTCA, the maximum rate is 0.176°C.s^{-1}, two orders of magnitude greater.

The onset of temperature rise occurs faster in the CTCA test. This highlights that the climate chamber system is limited by the response time of its control system. Using heaters to

change the temperature of the air used for convection cooling then moving the warmer air over the surface of the cell, is ultimately a slow method to induce temperature change in the cell. The CTCA, which directly cools the cell surface through conduction in copper plates, is able to effectively tackle this limitation.

The cell OCV may only be measured when the cell is held at the desired temperature for a prolonged period of time, in order for a thermal equilibrium state to be reached throughout the body of the cell. The test procedure to parameterise the entropy change in a lithium-ion cell, introduced by Zhao *et al.* [16], [31], can be optimised with the captured data. Conservatively, it is assumed in the following that the cell surface temperature must sit inside the threshold of $\Delta T < 0.25°C$ for 30 minutes, to ensure the entire volume of the cell has reached a sufficient state of thermal equilibrium. Table 4 summarises the procedure, in terms of time taken, with the original rest period of four hours, and for the required rest periods lengths when the test is optimised in the climate chamber and the CTCA. The superior performance of the CTCA dramatically reduces the time to reach the desired temperature for measurement. Across the entire experimental procedure, a time saving of 9.6 days is predicted when the CTCA is used instead of the climate chamber.

Driving Cycle Testing

The driving cycle tests are used to examine the CTCA's capability to maintain isothermal cell surface conditions when the rate of heat generation from the cell is significant and changes rapidly and randomly. The cell surface temperature rise recorded in each of the four tests is plotted in Figure 13, along with the power output for reference. The CTCA is able to maintain the desired surface temperature in both tests, whereas temperature rise is apparent in the climate chamber tests. The isothermal conditions reported from the CTCA test verify that the CTCA control system has a sufficiently rapid response time to deal with rapid changes to heat generation from within the cell under test. The performance at 5°C and 25°C highlight that the control system is not affected by absolute temperature. As with the pulse discharge

16

comparisons, the poor performance of the climate chamber is more apparent at low temperatures, where cell heat generation is greater.

The isothermal conditions achieved by the CTCA are not likely to be achievable in a full-scale battery pack, using the thermal management systems seen in the H/EV industry today. However, in achieving an isothermal boundary condition on a single cell, a battery modeller is able to decouple the effect of absolute temperature change during battery model parameterization. This is the greatest limitation of the climate chamber, as temperature fluctuation and achievable cooling rates are insufficient to allow isothermal boundary conditions to be used in a battery model. Climate chambers are able to simulate single cell cooling quite effectively but are unable to accurately represent the confinement of cells that would be expected in a H/EV battery pack.

Conclusions

The conductive thermal control apparatus is introduced as equipment to improve thermal control during lithium-ion cell experimentation in the H/EV industry. The CTCA cools the surface of test cells through conduction rather than convection. Conductive cooling is able to dramatically increase heat removal capability and thermal control. This is critical for the lithium-ion cell's of today, which can generate significant heat rates in high cycle-rate experiments.

The CTCA is able to maintain true isothermal cell surface conditions when a driving cycle, causing significant heat generation, is implemented onto a test cell. This is achievable from the rapid response of the control system and its ability to remove sufficient heat from a cell surface. Climate chamber control systems are unable to respond at the rate required, and forced convection is unable to achieve the required rates of heat removal. As a result, cell temperature fluctuation occurs in the climate chamber experiments. The more exaggerated

failure of the climate chamber's performance at low temperatures was expected because cell heat generation was greater.

Temperature rise occurs during climate chamber pulse discharge parameterization, and this affects the nature of the voltage relaxation following each pulse. This is caused by the cell impedance dependency on absolute temperature. The CTCA, by maintaining isothermal conditions on the cell surface through pulse discharge parameterization, is able to reduce the unknown effect of absolute cell temperature change.

The climate chamber requires an average of 84 minutes to achieve a 5°C temperature change of the cell surface. The CTCA requires just 1.6 minutes, a 98% saving. As a result, the CTCA can reduce the time taken to conduct a typical entropy parameterization procedure by 70%.

The results from the presented study provide strong evidence to suggest that climate chambers, which are used across the H/EV industry, are unable to effective control temperature during battery parameterization experiments. Implementation of conduction cooling during experimentation, for example using the CTCA, will require a more complex and timely apparatus setup. However, the time savings that may be made during experimentation and the enhancement to the quality of the data gathered will contribute to advancement of future battery models in the H/EV industry. Further testing is required on the CTCA, in order to optimise the parameterization procedures, set out in this study, and fully understand the impact that the move away from the climate chamber tests has on battery modelling.

References

[1]   Transparency Market Research, "Lithium-ion Battery Market (Product: Cells/ Modules, Battery Packs, and Energy Storage Systems (ESS); End-user Industry: Consumer Electronics, Automotive, and Grid Energy & Industrial) - Global Industry Analysis,

Size, Share, Growth, Trends, and Forecast," 2019. [Online]. Available:

https://www.transparencymarketresearch.com/lithium-ion-battery-market.html.

[2]   International Energy Agency, "World Energy Outlook 2019." 2019, [Online]. Available:

https://iea.blob.core.windows.net/assets/1f6bf453-3317-4799-ae7b-

9cc6429c81d8/English-WEO-2019-ES.pdf.

[3]   G. Zubi, R. Dufo-lópez, M. Carvalho, and G. Pasaoglu, "The lithium-ion battery : State

of the art and future perspectives," *Renew. Sustain. Energy Rev.*, vol. 89, no. October

2017, pp. 292–308, 2018, doi: 10.1016/j.rser.2018.03.002.

[4]   T. Lieven, "Policy measures to promote electric mobility – A global perspective,"

Transp. Res. Part A Policy Pract., vol. 82, pp. 78–93, Dec. 2015, doi:

10.1016/J.TRA.2015.09.008.

[5]   J. H. M. Langbroek, J. P. Franklin, and Y. O. Susilo, "The effect of policy incentives on

electric vehicle adoption," *Energy Policy*, vol. 94, pp. 94–103, Jul. 2016, doi:

10.1016/J.ENPOL.2016.03.050.

[6]   M. Contestabile, M. Alajaji, and B. Almubarak, "Will current electric vehicle policy lead

to cost-effective electrification of passenger car transport?," *Energy Policy*, vol. 110,

pp. 20–30, Nov. 2017, doi: 10.1016/J.ENPOL.2017.07.062.

[7]   A. Fotouhi, D. J. Auger, K. Propp, S. Longo, and M. Wild, "A review on electric vehicle

battery modelling: From Lithium-ion toward Lithium–Sulphur," *Renew. Sustain. Energy

Rev.*, vol. 56, pp. 1008–1021, Apr. 2016, doi: 10.1016/J.RSER.2015.12.009.

[8]   S. M. Mousavi G. and M. Nikdel, "Various battery models for various simulation

studies and applications," *Renew. Sustain. Energy Rev.*, vol. 32, pp. 477–485, Apr.

2014, doi: 10.1016/J.RSER.2014.01.048.

[9]   X. Zhang, W. Zhang, and G. Lei, "A review of li-ion battery equivalent circuit models,"

Trans. Electr. Electron. Mater., vol. 17, no. 6, pp. 311–316, 2016, doi:

10.4313/TEEM.2016.17.6.311.

[10]   P. Haussmann and J. Melbert, "Internal Cell Temperature Measurement and Thermal Modeling of Lithium Ion Cells for Automotive Applications by Means of Electrochemical Impedance Spectroscopy," *SAE Int. J. Altern. Powertrains*, vol. 6, no. 2, May 2017, [Online]. Available: http://www.jstor.org/stable/26169169.

[11]   A. A. Pesaran, "Battery thermal models for hybrid vehicle simulations," *J. Power Sources*, vol. 110, no. 2, pp. 377–382, Aug. 2002, doi: 10.1016/S0378-7753(02)00200-8.

[12]   M. I. Ardani, Y. Patel, A. Siddiq, G. J. Offer, and R. F. Martinez-Botas, "Combined experimental and numerical evaluation of the differences between convective and conductive thermal control on the performance of a lithium ion cell," *Energy*, vol. 144, pp. 81–97, 2018, doi: 10.1016/j.energy.2017.12.032.

[13]   Y. Troxler *et al.*, "The effect of thermal gradients on the performance of lithium-ion batteries," *J. Power Sources*, vol. 247, pp. 1018–1025, 2014, doi: 10.1016/j.jpowsour.2013.06.084.

[14]   Y. Xie, S. Shi, J. Tang, H. Wu, and J. Yu, "Experimental and analytical study on heat generation characteristics of a lithium-ion power battery," *Int. J. Heat Mass Transf.*, vol. 122, pp. 884–894, 2018, doi: 10.1016/j.ijheatmasstransfer.2018.02.038.

[15]   B. Wu, V. Yufit, M. Marinescu, G. J. Offer, R. F. Martinez-Botas, and N. P. Brandon, "Coupled thermal-electrochemical modelling of uneven heat generation in lithium-ion battery packs," *J. Power Sources*, vol. 243, pp. 544–554, 2013, doi: 10.1016/j.jpowsour.2013.05.164.

[16]   Y. Zhao, Y. Patel, T. Zhang, and G. J. Offer, "Modeling the Effects of Thermal Gradients Induced by Tab and Surface Cooling on Lithium Ion Cell Performance," *J. Electrochem. Soc.*, vol. 165, no. 13, pp. A3169–A3178, 2018, doi:

10.1149/2.0901813jes.

[17] R. Rizk, H. Louahlia, H. Gualous, and P. Schaetzel, "Experimental analysis and transient thermal modelling of a high capacity prismatic lithium-ion battery," *Int. Commun. Heat Mass Transf.*, vol. 94, pp. 115–125, 2018, doi: 10.1016/J.ICHEATMASSTRANSFER.2018.03.018.

[18] W. B. Gu and C. Y. Wang, "Thermal-Electrochemical Modeling of Battery Systems," *J. Electrochem. Soc.*, vol. 147, no. 8, pp. 2910–2923, 2000.

[19] T. M. Bandhauer, S. Garimella, and T. F. Fuller, "Temperature-dependent electrochemical heat generation in a commercial lithium-ion battery," *J. Power Sources*, vol. 247, pp. 618–628, 2014, doi: 10.1016/j.jpowsour.2013.08.015.

[20] G. J. Offer, V. Yufit, D. A. Howey, B. Wu, and N. P. Brandon, "Module design and fault diagnosis in electric vehicle batteries," *J. Power Sources*, vol. 206, pp. 383–392, May 2012, doi: 10.1016/J.JPOWSOUR.2012.01.087.

[21] S. Mazyar and H. Moghaddam, "Designing battery thermal management systems(BTMS) for cylindrical Lithium-ion battery modules using CFD," KTH School of Industrial Engineering and Management, 2019.

[22] A. Jossen, V. Spath, H. Doring, and J. Garche, "Battery management systems (BMS) for increasing battery life time," in *21st International Telecommunications Energy Conference. INTELEC '99 (Cat. No.99CH37007)*, 1999, p. 56, doi: 10.1109/INTLEC.1999.794018.

[23] N. A. Chaturvedi, R. Klein, J. Christensen, J. Ahmed, and A. Kojic, "Algorithms for Advanced Battery-Management Systems," *IEEE Control Syst. Mag.*, vol. 30, no. 3, pp. 49–68, 2010, doi: 10.1109/MCS.2010.936293.

[24] B. Schleich, N. Anwer, L. Mathieu, and S. Wartzack, "Shaping the digital twin for design and production engineering," *CIRP Ann.*, vol. 66, no. 1, pp. 141–144, Jan.

2017, doi: 10.1016/J.CIRP.2017.04.040.

[25] S. Du *et al.*, "An investigation of irreversible heat generation in lithium ion batteries based on a thermo-electrochemical coupling method," *Appl. Therm. Eng.*, vol. 121, pp. 501–510, 2017, doi: 10.1016/j.applthermaleng.2017.04.077.

[26] R. Ahmed *et al.*, "Model-Based Parameter Identification of Healthy and Aged Li-ion Batteries for Electric Vehicle Applications," *SAE Int. J. Altern. Powertrains*, vol. 4, no. 2, pp. 233–247, May 2015, [Online]. Available: http://www.jstor.org/stable/26169083.

[27] A. Cordoba-Arenas, S. Onori, and G. Rizzoni, "A control-oriented lithium-ion battery pack model for plug-in hybrid electric vehicle cycle-life studies and system design with consideration of health management," *J. Power Sources*, vol. 279, pp. 791–808, Apr. 2015, doi: 10.1016/J.JPOWSOUR.2014.12.048.

[28] J. Taylor, A. Barai, T. R. Ashwin, Y. Guo, M. Amor-Segan, and J. Marco, "An insight into the errors and uncertainty of the lithium-ion battery characterisation experiments," *J. Energy Storage*, vol. 24, p. 100761, 2019, doi: https://doi.org/10.1016/j.est.2019.100761.

[29] M. Ecker, T. K. D. Tran, P. Dechent, S. Kabitz, A. Warnecke, and D. U. Sauer, "Parameterization of a Physico-Chemical Model of a Lithium-Ion Battery: I. Determination of Parameters," *J. Electrochem. Soc.*, vol. 162, no. 9, pp. A1836–A1848, 2015, doi: 10.1149/2.0551509jes.

[30] M. Ecker, S. Käbitz, I. Laresgoiti, and D. U. Sauer, "Parameterization of a Physico-Chemical Model of a Lithium-Ion Battery," *J. Electrochem. Soc.*, vol. 162, no. 9, pp. A1849–A1857, 2015, doi: 10.1149/2.0541509jes.

[31] Y. Zhao, L. B. Diaz, and G. J. Offer, "How to Cool Lithium Ion Batteries : Optimising Cell Design using a Thermally Coupled Model," *J. Electrochem. Soc.*, vol. 166, no. 13, pp. 2849–2859, 2019, doi: 10.1149/2.0501913jes.

[32]   A. Li, S. Pelissier, P. Venet, and P. Gyan, "Fast characterization method for modeling battery relaxation voltage," *Batteries*, vol. 2, no. 2, 2016, doi: 10.3390/batteries2020007.

[33]   D. Bernardi, "A General Energy Balance for Battery Systems," *J. Electrochem. Soc.*, vol. 132, no. 1, p. 5, 1985, doi: 10.1149/1.2113792.

[34]   K. E. Thomas and J. Newman, "Heats of mixing and of entropy in porous insertion electrodes," *J. Power Sources*, vol. 119–121, pp. 844–849, 2003, doi: 10.1016/S0378-7753(03)00283-0.

[35]   European Automobile Manufacturers Association, "Getting Ready for WLTP," 2017. https://www.wltpfacts.eu/what-is-wltp-how-will-it-work/ (accessed Jun. 04, 2020).

[36]   M. Khan, M. Swierczynski, and S. Kær, "Towards an Ultimate Battery Thermal Management System: A Review," *Batteries*, vol. 3, no. 4, p. 9, Mar. 2017, doi: 10.3390/batteries3010009.

[37]   C. Lin *et al.*, "Comparative study on the heat generation behavior of lithium-ion batteries with different cathode materials using accelerating rate calorimetry," *Energy Procedia*, vol. 142, pp. 3369–3374, 2017, doi: 10.1016/j.egypro.2017.12.472.

[38]   C. Lin, S. Xu, and J. Liu, "Measurement of heat generation in a 40 Ah LiFePO4prismatic battery using accelerating rate calorimetry," *Int. J. Hydrogen Energy*, vol. 43, no. 17, pp. 8375–8384, 2018, doi: 10.1016/j.ijhydene.2018.03.057.

[39]   A. Hales, M. W. Marzook, L. Bravo Diaz, Y. Patel, and G. Offer, "The Surface Cell Cooling Coefficient: A Standard to Define Heat Rejection from Lithium Ion Battery Pouch Cells," *J. Electrochem. Soc.*, vol. 167, no. 2, p. 020524, 2020, doi: 10.1149/1945-7111/ab6985.

[40]   O. Dondelewski *et al.*, "The role of cell geometry when selecting tab or surface cooling to minimise cell degradation," *eTransportation*, 2020.

[41] D. Li and L. Yang, "Identification of spatial temperature gradient in large format lithium battery using a multilayer thermal model," *Int. J. Energy Res.*, vol. 44, no. 1, pp. 282–297, Jan. 2020, doi: 10.1002/er.4914.

[42] H. Dai, B. Jiang, and X. Wei, "Impedance Characterization and Modeling of Lithium-Ion Batteries Considering the Internal Temperature Gradient," *Energies*, vol. 11, no. 1, p. 220, Jan. 2018, doi: 10.3390/en11010220.

[43] T. Waldmann *et al.*, "Influence of Cell Design on Temperatures and Temperature Gradients in Lithium-Ion Cells: An In Operando Study," *J. Electrochem. Soc.*, vol. 162, no. 6, pp. A921–A927, 2015, doi: 10.1149/2.0561506jes.

[44] BINDER, "BINDER Model KB 53 | Datasheet." 2020.

[45] Vehicle Certification Agnecy, "The Worldwide Harmonised Light Vehicle Test Procedure (WLTP)." https://www.vehicle-certification-agency.gov.uk/fcb/wltp.asp (accessed Jul. 24, 2020).

[46] A. O. Kıyaklı and H. Solmaz, "Modeling of an Electric Vehicle with MATLAB/Simulink," *Int. J. Automot. Sci. Technol.*, vol. 2, no. 4, pp. 9–15, Jan. 2019, doi: 10.30939/ijastech..475477.

[47] D. J. Auger, "Driving Cycle (Simulink Block)." MATLAB Central File Exchange, 2020, [Online]. Available: https://www.mathworks.com/matlabcentral/fileexchange/46777-driving-cycle-simulink-block.

[48] L. Guzzella and A. Sciarretta, *Vehicle Propulsion Systems: Introduction to Modeling and Optimization.* 2007.

Acknowledgements

Conflict of Interest Disclosure

In accordance with our ethical obligation as researchers, we are declaring that the experiments detailed in this investigation were conducted as part of the Innovate UK THT project (grant number 105297). We have fully disclosed our interests to SAE International.

Appendix A

This appendix contains the temperature rise magnitudes and temperature rise settling times

for each pulse discharge test conducted in the climate chamber.
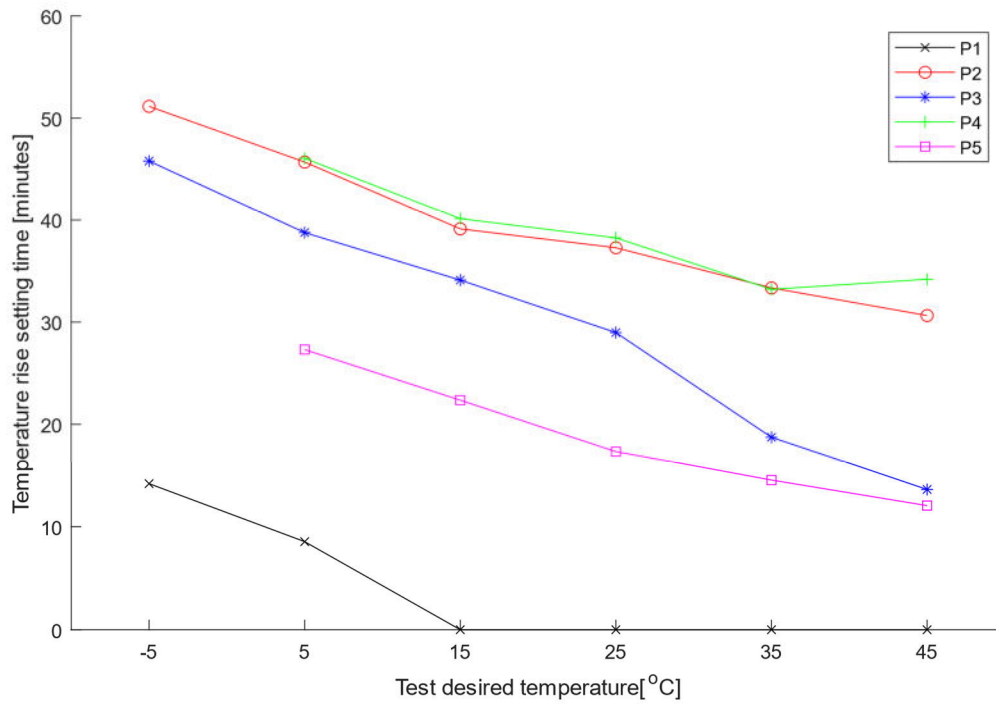
A 1: Temperature rise settling time for each climate chamber experiment conducted as part of the pulse discharge testing
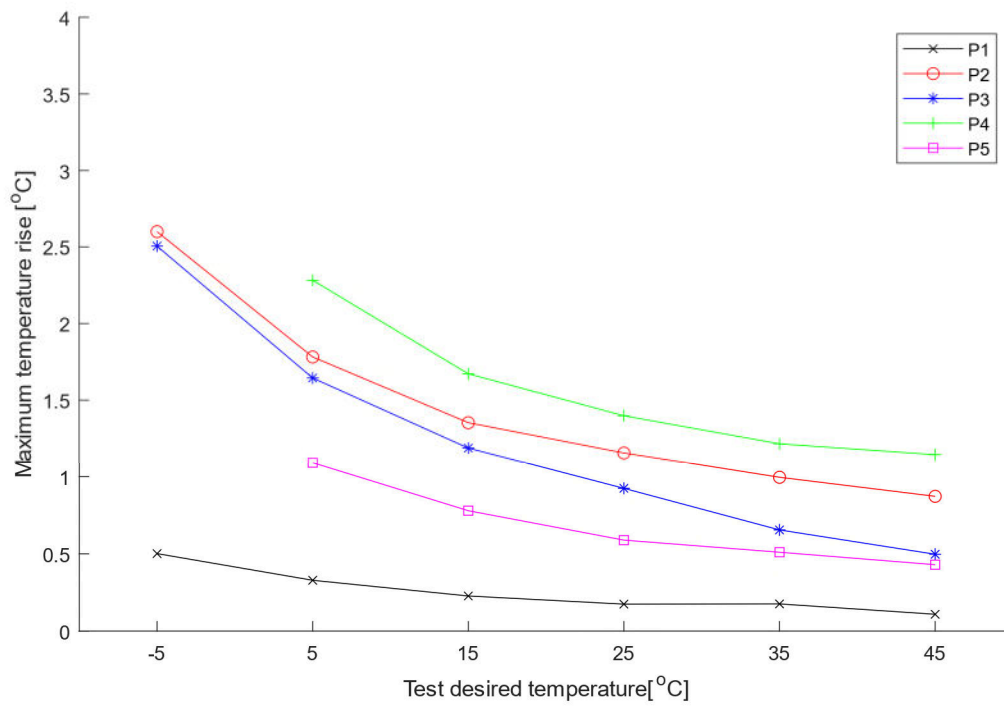
A 2: Maximum temperature rise for each climate chamber experiment conducted as part of the pulse discharge testing

Appendix B

This appendix contains the *dV/dt* settling time for each experiment conducted as part of the pulse discharge testing.

A 3: *dV/dt* settling time for each climate chamber experiment conducted as part of the pulse discharge testing

Test temperature	*dV/dt* settling time [minutes]				
	P1	**P2**	**P3**	**P4**	**P5**
	100% - 99% SOC	**90% - 85% SOC**	**55% - 50% SOC**	**25% - 20% SOC**	**17% - 15% SOC**
-5°C	29.6	61.0	65.2	n/a	n/a
5°C	25.3	44.1	49.5	44.9	37.5
15°C	23.2	37.2	39.6	36.5	30.6
25°C	20.5	31.8	37.5	31.9	25.3
35°C	18.9	27.6	34.8	28.5	22.9
45°C	18.4	23.6	32.0	25.4	21.5

A 4: *dV/dt* settling time for each CTCA experiment conducted as part of the pulse discharge testing

Test temperature	*dV/dt* settling time [minutes]				
	P1	**P2**	**P3**	**P4**	**P5**
	100% - 99% SOC	**90% - 85% SOC**	**55% - 50% SOC**	**25% - 20% SOC**	**17% - 15% SOC**
-5°C	30.1	74.7	69.9	n/a	n/a
5°C	24.9	52.9	51.8	51.8	37.2
15°C	22.1	41.5	42.0	39.3	30.0
25°C	20.7	32.9	35.0	32.5	26.4
35°C	19.3	28.0	36.6	28.7	24.0
45°C	18.2	24.8	32.7	25.9	22.2

Appendix C

This appendix contains the temperature deviation settling time for each experiment conducted as part of the temperature step change testing.

A 5: Temperature deviation settling time for each climate chamber experiment conducted as part of the temperature step change testing

Start temperature [°C]	Target temperature [°C]	Settling time [minutes]
15	20	104.0
20	25	89.0
25	30	74.8
30	35	81.4
35	40	79.0
40	35	76.5
35	30	87.2
30	25	83.4
25	20	81.9
20	15	84.1
15	40	131.9
40	15	139.8

A 6: Temperature deviation settling time for each CTCA experiment conducted as part of the temperature step change testing

Start temperature [°C]	Target temperature [°C]	Settling time [minutes]
15	20	1.3
20	25	1.6
25	30	1.3
30	35	1.7
35	40	1.7
40	35	1.7
35	30	1.5
30	25	1.8
25	20	1.5
20	15	1.2
15	40	3.0
40	15	3.9

Figures
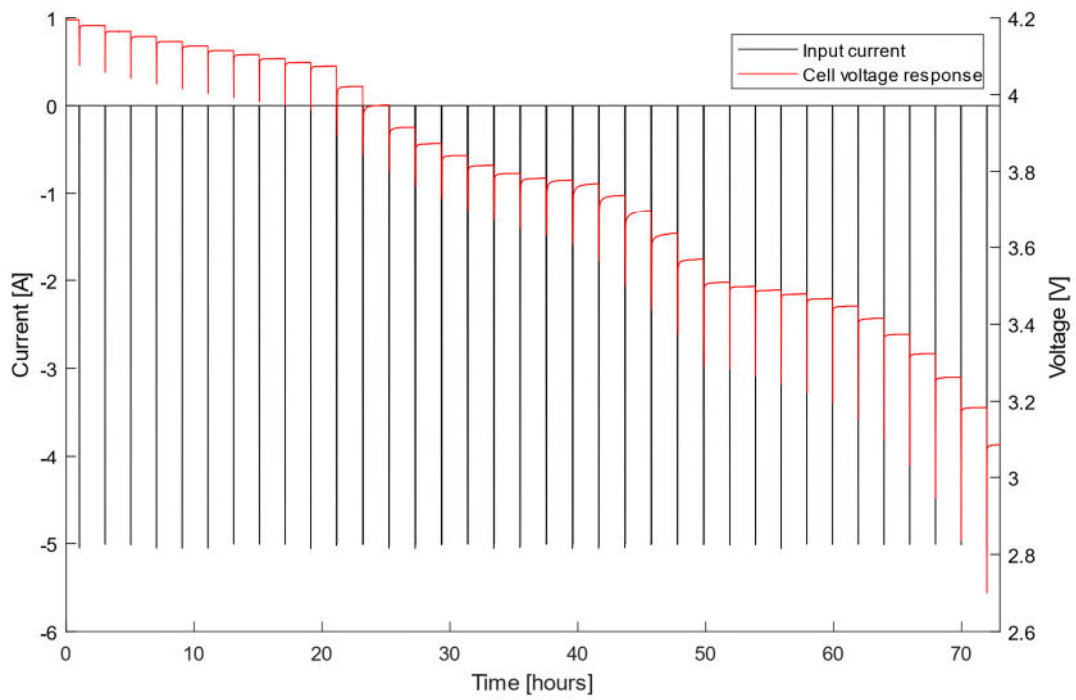
Figure 1: Pulse discharge test results for a 5Ah Kokam pouch cell. Data taken from Ref. [16]
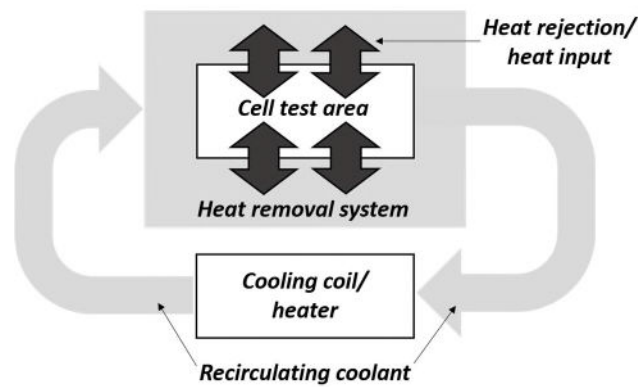
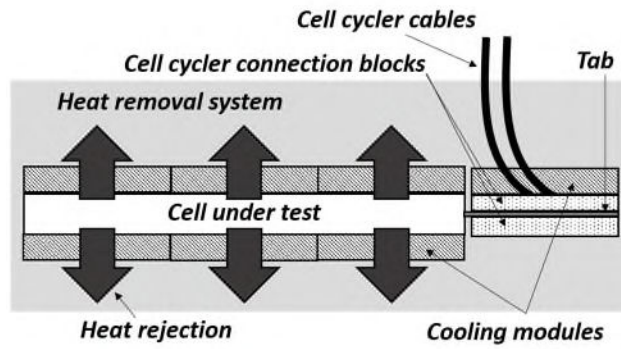**Figure 2: High-level schematic of conductive thermal control apparatus**

Figure 3: Schematic of test area within the assembly of the conductive thermal control apparatus
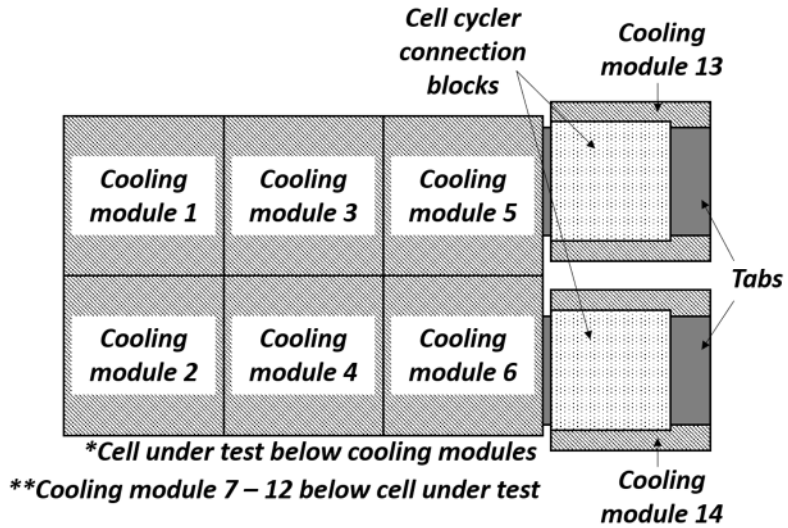

*Cell under test below cooling modules
**Cooling module 7 – 12 below cell under test

Figure 4: Layout of cooling modules used for testing on large format pouch cell
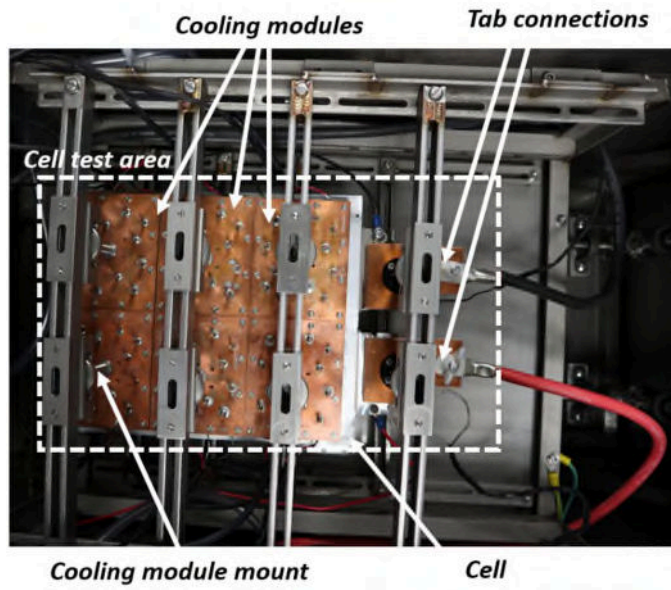
Figure 5: Image of the test cell setup within the Cell Test Area of the CTCA. NB: during testing, the cell test area is immersed in the coolant fluid. Not shown here for clarity of image
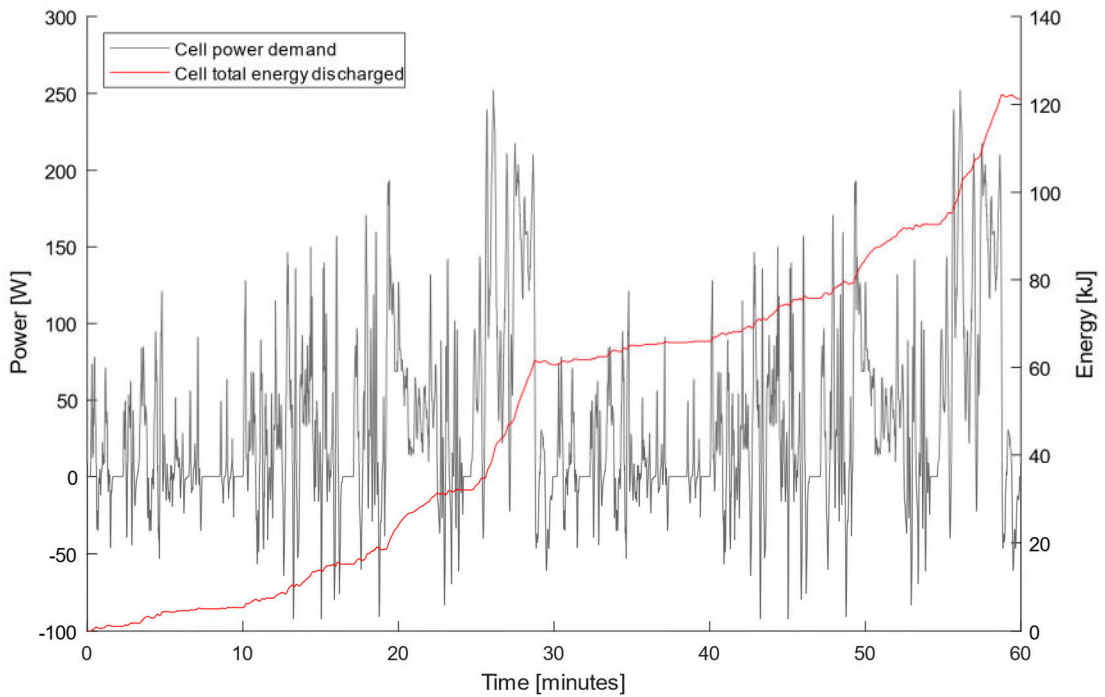

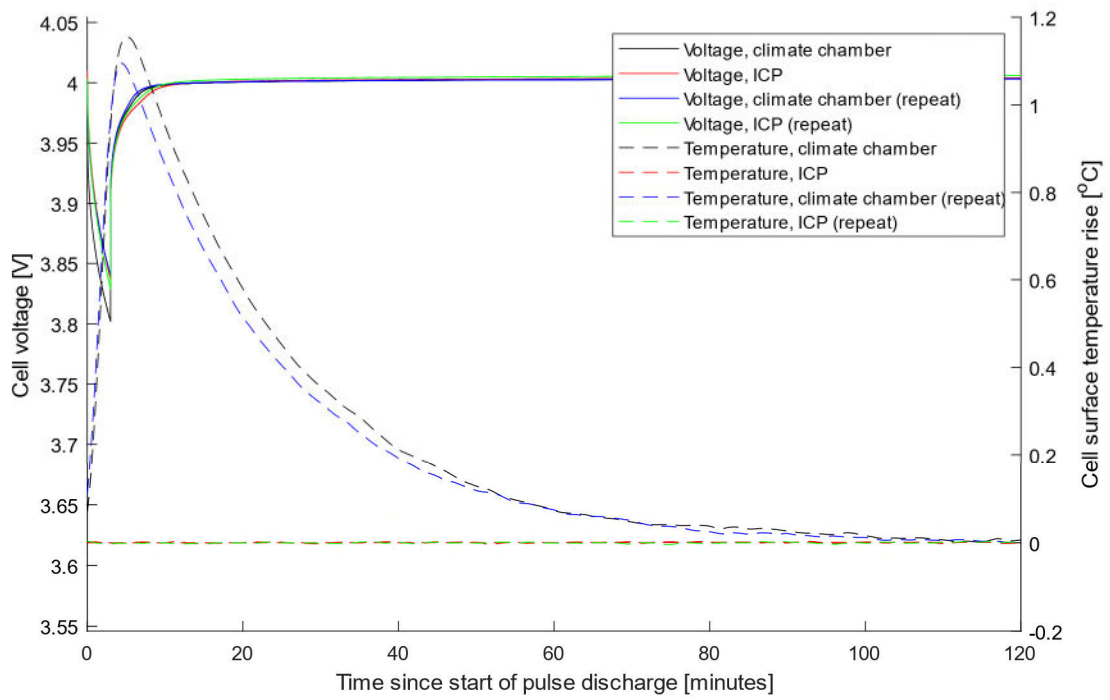**Figure 6: WLTP power-rated load on a 56Ah cell when contained within a 40kWh battery pack**

Figure 7: Cell voltage response and temperature rise following pulse discharge, 90% - 85% SOC (P2), at 25°C in the climate chamber and CTCA
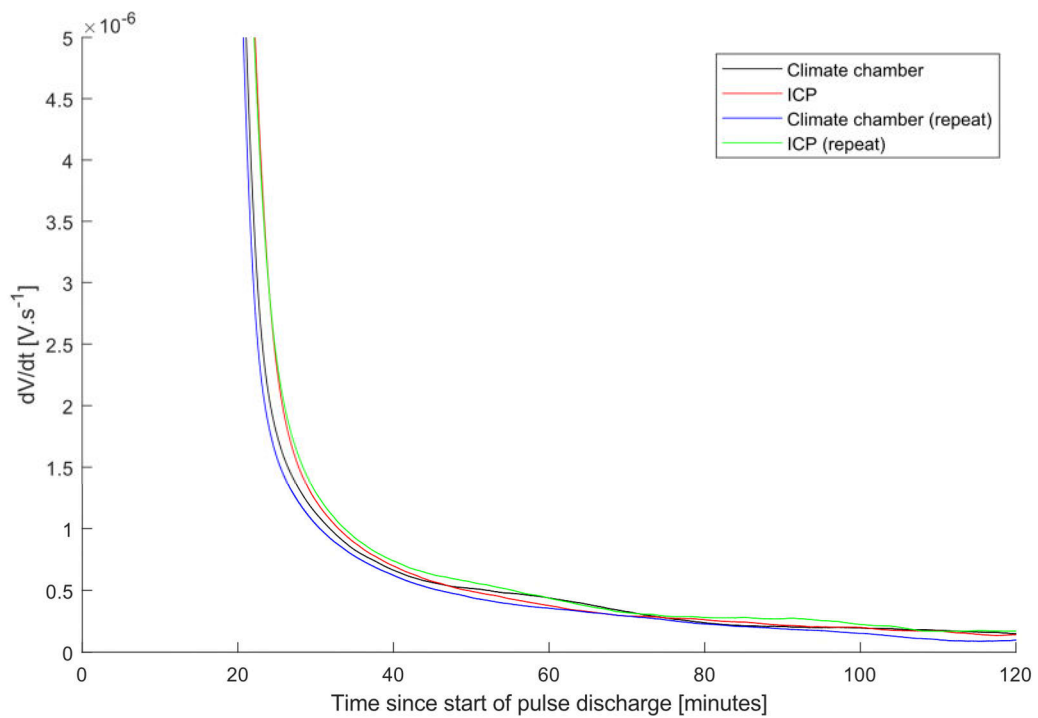

Figure 8: *dV/dt* response following pulse discharge, 90% - 85% SOC (P2), at 25°C in the climate chamber and CTCA
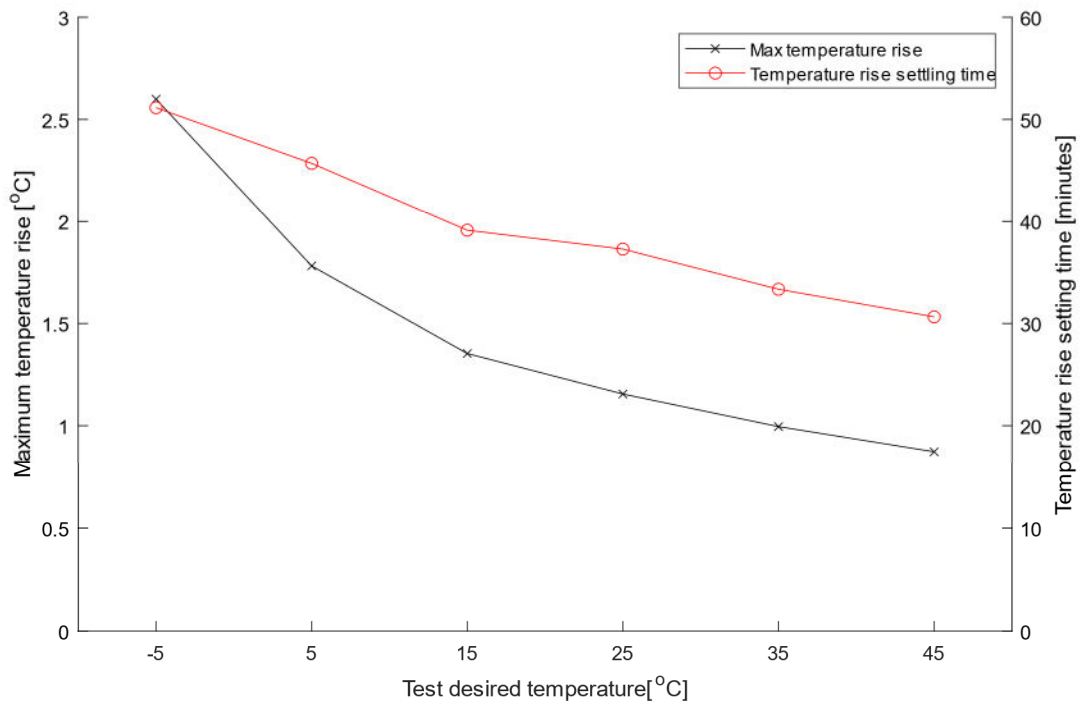
Figure 9: The maximum temperature rise and the temperature setting time following pulse discharge, 90% - 85% SOC (P2), at each test temperature in the climate chamber
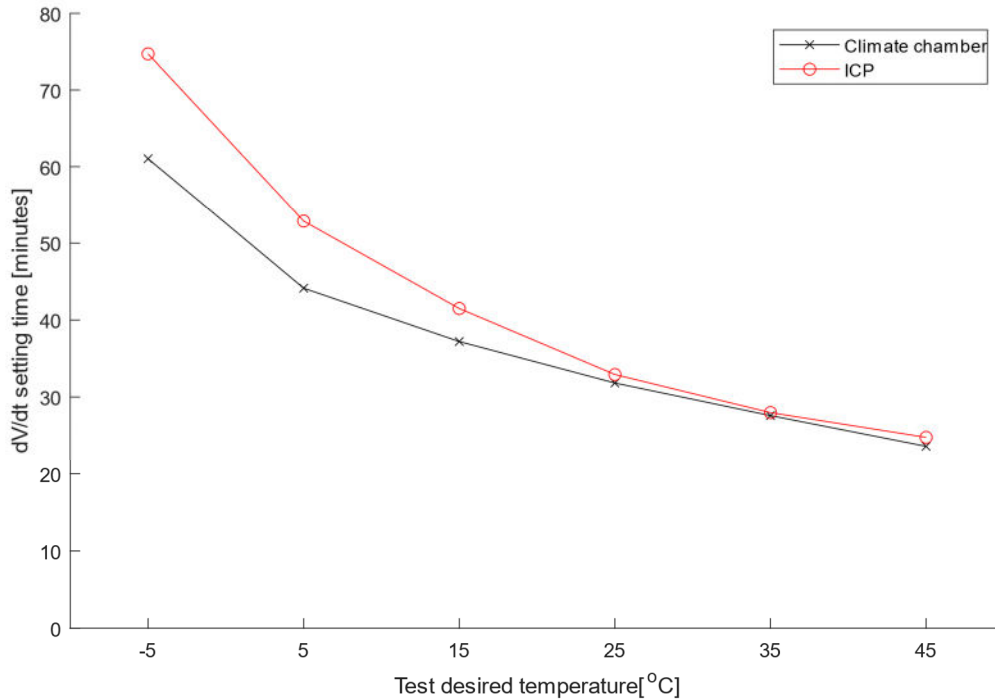

Figure 10: *dV/dt* **settling time following pulse discharge, 90% - 85% SOC (P2), at each test temperature in the climate chamber and CTCA**
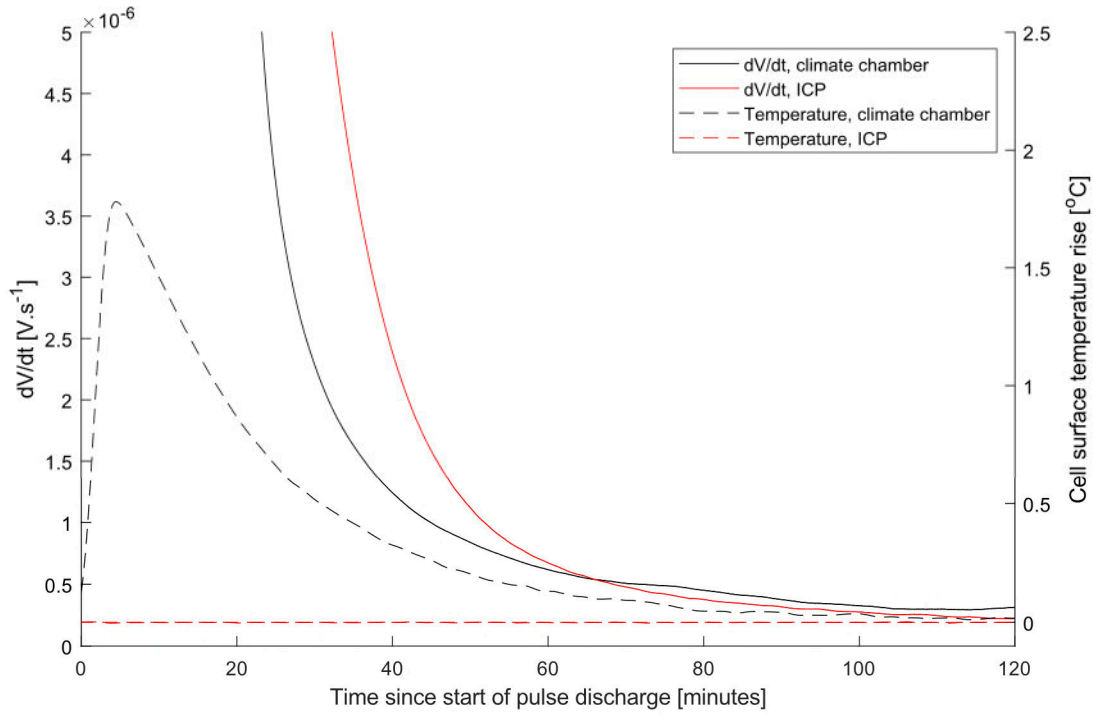
Figure 11: *dV/dt* **response and temperature rise following pulse discharge, 25% - 20% SOC (P4), at 5°C in the climate chamber and CTCA**
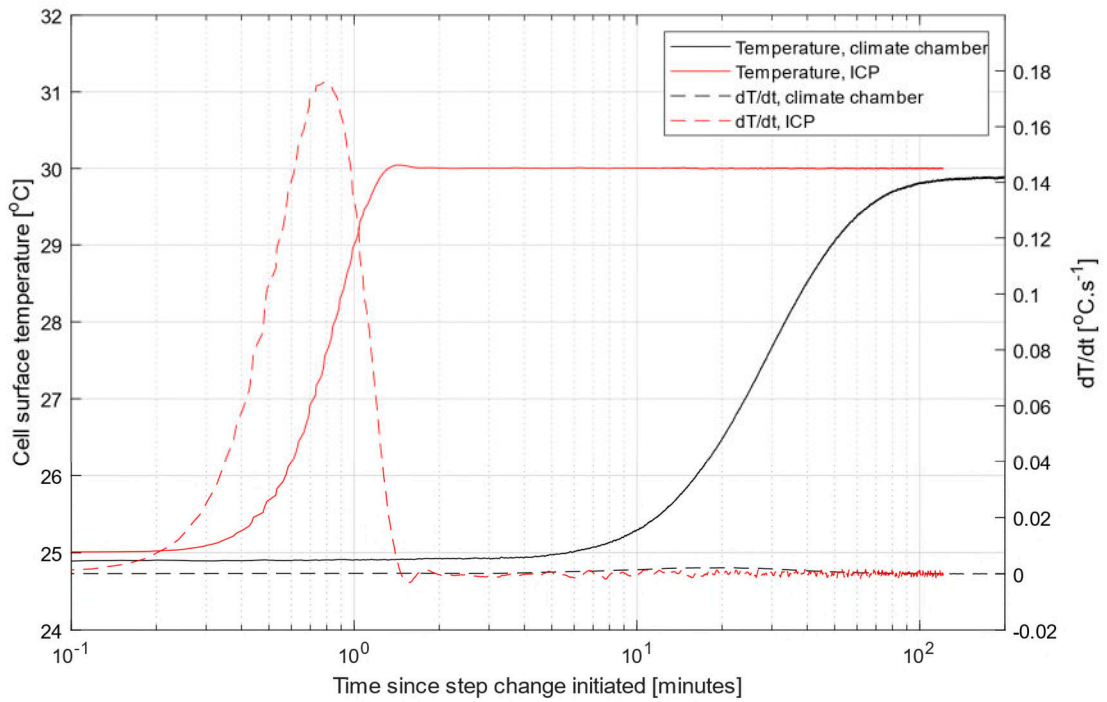

Figure 12: Temperature step-change (35°C - 40°C) and voltage response in the climate chamber and CTCA
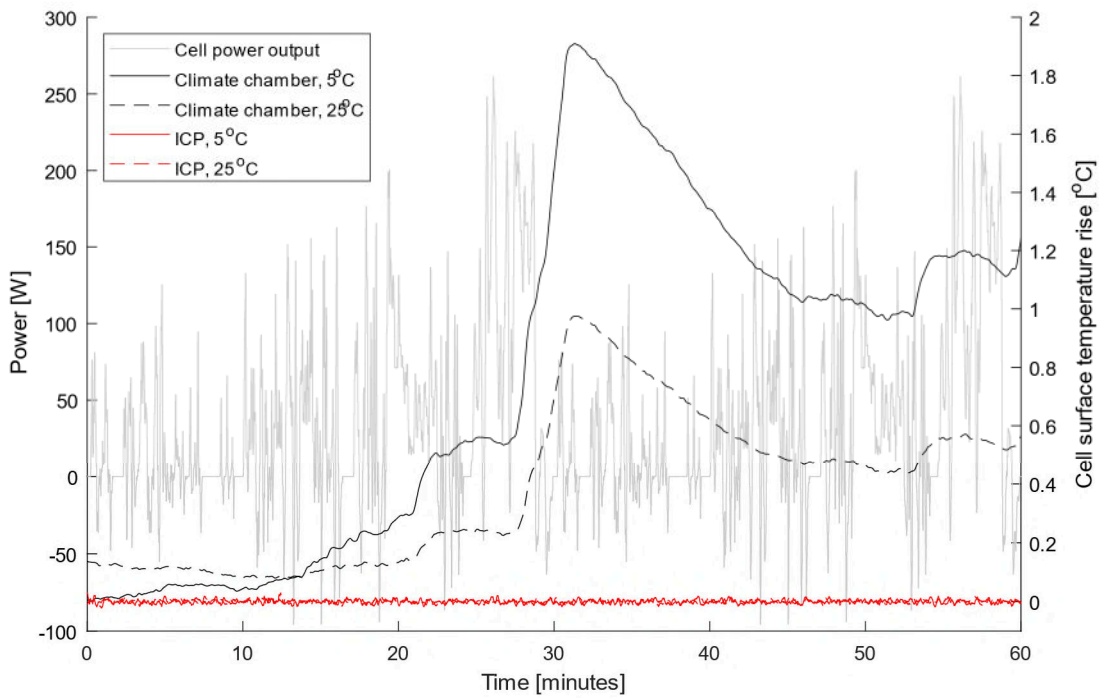
Figure 13: Cell surface temperature rise in all four tests (5°C and 25°C, climate chamber and CTCA) over the course of the WLTP driving cycle (calculated based on 56Ah cell contained within a 40kWh battery pack)

Tables

Table 1: Selected climate chamber performance results found. Data taken from Ref [12]

Desired Temperature/ °C	Maximum temperature deviation/ °C		Reduction of error through conduction
	Climate chamber	Conduction apparatus	
45	2.4	0.6	75%
35	2.5	0.7	72%
25	3.7	0.9	76%
15	4.6	1.0	78%
5	5.7	1.2	79%

Table 2: Pulse discharge testing matrix. Y = test conducted in CTCA and in climate chamber. *NB: in the climate chamber and the CTCA tests, the cell lower voltage cut-off (2.5V) was reached before these pulse discharges could be completed

Pulse name	P1	P2	P3	P4	P5
SOC change:	100% - 99%	90% - 85%	55% - 50%	25% - 20%	17% - 15%
-5°C	Y	Y	Y	Y*	Y*
5°C	Y	Y	Y	Y	Y
15°C	Y	Y	Y	Y	Y
25°C	Y	Y	Y	Y	Y

35°C	Y	Y	Y	Y	Y
45°C	Y	Y	Y	Y	Y

Table 3: Temperature step change testing matrix. Y = test conducted in CTCA and in climate chamber

Start temp [°C] / Finish temp[°C]	15	20	25	30	35	40
15	N	Y	N	N	N	Y
20	Y	N	Y	N	N	N
25	N	Y	N	Y	N	N
30	N	N	Y	N	Y	N
35	N	N	N	Y	N	Y
40	Y	N	N	N	Y	N

Table 4: Entropy test procedure presented by Zhao *et al.* and optimised to reflect response times of temperature control system in the present investigation. Data taken from Ref. [16]

Step	Mode		Time for step [minutes]		
			Zhao *et al*	Climate chamber	CTCA
2	Temperature step change	40°C - 15°C	240	140	3.9
3	Discharge (C/20)	4% ∆SOC	48	48	48
4	Rest	OCV record	240	30	30
5	Temperature step change	15°C - 20°C	n/a	104	1.3
6	Rest	OCV record	240	30	30
5	Temperature step change	20°C - 25°C	n/a	89	1.6
6	Rest	OCV record	240	30	30
5	Temperature step change	25°C -30°C	n/a	75	1.3
6	Rest	OCV record	240	30	30
5	Temperature step change	30°C - 35°C	n/a	81	1.7
6	Rest	OCV record	240	30	30
5	Temperature step change	35°C - 40°C	n/a	79	1.7
6	Rest	OCV record	240	30	30
Return to step 2 until 0% SOC reached (25 loops in total)					
Total time [days]:			**30**	**13.8**	**4.2**